ELSEVIER

Pressure drop coefficient of laminar Newtonian flow in axisymmetric sudden expansions

P. J. Oliveira
Departamento de Engenharia Electromecânica, Universidade de Beira Interior, Covilhã, Portugal

F. T. Pinho
Departamento de Engenharia Mecânica, Faculdade de Engenharia, Porto, Portugal

Laminar flow of a Newtonian fluid in an axisymmetric pipe expansion has been studied numerically by means of the finite-volume approach. Predicted values of some of the overall flow characteristics, such as recirculation length, its strength, and centre location, were compared with available experimental data and correlations, and good agreement was found. The purpose of the work was to evaluate the pressure-loss coefficient C_1 for a range of Reynolds numbers and to compare the results with existing simplified theory, which is based on a one-dimensional (1-D) overall balance of energy and momentum. Considerable differences were found, which lead us to formulate corrected theoretical equations in the scope of the 1-D approximation. These corrections were evaluated from the numerical results and accounted for three effects: (1) differing actual and fully developed wall friction; (2) distortion of velocity profiles from the parabolic shape at the sudden expansion section; and (3) nonuniformity of pressure at the expansion plane. Predicted values of the loss coefficient agreed to within 4% with the corrected theory and were found to be proportional to the inverse of the Reynolds number for $Re \leq 17.5$ [with effect (3) above predominant and accounting for up to 85% of C_f] and approximately constant for $Re > 17.5$ [with effect (1) above predominant and accounting for 20% of C_f]. Finally, a correlation for calculating the local loss coefficient as a function of the Reynolds number for the 1:2.6 sudden expansion and fully developed conditions is proposed.

Keywords: sudden expansion; loss coefficient; laminar flow

Introduction

Sudden expansion flows bring together geometric simplicity with a complex flow behavior because of the interaction of a recirculation region and a jet in a confined duct, but their relevance also stems from the fact that they often occur in industry. This type of flow has been thoroughly investigated in the past both numerically (Macagno and Hung 1967; Habib and Whitelaw 1982; Fletcher *et al.* 1985) and experimentally (Macagno and Hung 1967; Back and Roshke 1972; Khezzar *et al.* 1985: Stieglmeier *et al.* 1989) amongst others, in the laminar and mainly in the turbulent flow regimes and, thus, provides a good configuration for testing experimental and numerical work. Some of the flow characteristics of the more recent work on low-Reynolds number flows are presented in Table 1, which is not meant to be an exhaustive listing.

Many applications of Newtonian sudden expansion flows pertain to the turbulent flow regime, because they involve low-viscosity fluids, such as air or water. Examples are ventilation flows (Restivo and Whitelaw 1979), flows of relevance to aeronautics (Abbott and Kline 1962), and to combustion (Drewry 1978). However, in many other instances, where high-viscosity fluids and/or tiny geometries are involved, as in glass melting, polymer processing flows, and some mixing flows, their characteristics can be laminar, as reported by McNaughton and Sinclair (1966), Tadmor and Gogos (1979), and Boger (1981).

Some of these industrial fluids are, indeed, more complex in rheology than the Newtonian constitutive equation is capable of predicting, but the focus on non-Newtonian behavior is left to another occasion, because some basic features of Newtonian laminar sudden expansion flows are still unknown and are required for an adequate understanding of the more complex fluid flow hydrodynamics of those fluids.

Proper assessment of pumping power in ducts requires knowledge of the friction and local losses in pipes and fittings. Only one of the references (Idel'cik, 1971) in Table 1 presents some information on local loss coefficients for laminar sudden expan-

Address reprint to Dr. F. T. Pinho, D.E.M.E.G.I., Faculty of Engineering, Rua dos Bragas, 4099 Porto Cedex, Portugal.

Received 29 June 1996; accepted 22 March 1997

Int. J. Heat and Fluid Flow 18: 518–529 (1997)

655 Avenue of the Americas, New York, NY 10010

0142-727X/97/$17.00
PII S0142-727X(97)00042-8

Table 1 Some publications on axisymmetric sudden expansion flows at low Reynolds numbers

Reference	Reynolds Number	Flow condition	Remarks
Macagno and Hung (1967)	Re = up to 200*	$D_2/D_1 = 2.0$	Exp. and Num.-FD
Back and Roshke (1972)	Re = 20 to 4200	$D_2/D_1 = 2.6$	Exp.-≈ U
Iribarne et al. (1972)	Re = 90 to 1355	$D_2/D_1 = 2.0$	Exp.-≈ U
Badekas and Knight (1992)	Re = 50 to 200	$D_2/D_1 = 1.5$ to 6.0	Compilation-FD
Stieglmeier et al. (1989)	Re = 15600	$D_2/D_1 = 1.6$	Exp.-FD
Idel'cik (1971)	Re ≤ 3500 and Re > 3500	D_2/D_1 = general	Compilation
Milos and Acrivos (1986)	Re → ∞ (Laminar)	D_2/D_1 = general	Theo.-U
Scott et al. (1986)	Re = 50 to 200	$D_2/D_1 = 1.5, 2.0, 3.0, 4.0$	Num.-FD
Monnet et al. (1982)	Re = 0.04 to 29.4	$D_2/D_1 = 2.26$	Exp.-FD

U-uniform inlet velocity profile; FD-fully developed inlet velocity profile; $Re = \rho D_1 \bar{u}_1/\mu$
*Flow visualizations up to 4500 were also carried out, but the detailed work went up to 200

sion flows, but it is limited to the case of a plug inlet velocity profile, with the remaining works concentrated on the measurement or prediction of other flow features, such as the recirculation bubble length, or its intensity. For low-Reynolds number laminar flows, the length of pipe required for flow development can be rather short, and fully developed flow is bound to occur frequently. Classical fluid dynamics textbooks and references such as Batchelor (1967), Idel'cik (1971), Streeter and Wylie (1975), or White (1979), emphasise the use of the theoretical local loss coefficient, which has been validated for turbulent flow, but is not correct in the laminar regime. Throughout this paper, we refer to such derivation as the standard theory. Therefore, the objective of this paper is to calculate the local loss coefficient in an axisymmetric sudden expansion, and to assess numerically its various contributions for the case of a Newtonian fluid with fully developed inlet flow conditions.

The next section presents the theory and definitions required in this work; it is followed by an outline of the numerical procedure, the specifications of the calculation domain, and the boundary conditions. The presentation and discussion of the

Notation

a	wetted perimeter area
A	cross section area
ΔC	corrective pressure coefficient
C_p	general pressure coefficient
D	pipe diameter
f	Darcy fraction factor
f_x, f_r	geometrical expansion factors ($= \delta_{i+1}/\delta_i$)
h	step height
L	length
NC	number of internal cells of computational grid
p	pressure
Δp	pressure difference
r	radial coordinate
R	pipe radius
Re	Reynolds number ($= \rho D_1 \bar{u}_1/\mu$)
u	axial velocity component
x	axial coordinate ($X = x/D_1$)
x_c	axial position of eddy centre ($X_c = x_c/D_1$)
x_r	recirculation length ($X_r = x_r/D_1$)
Y	height of the wedge-shaped computational domain
Z	half-size of the base of the wedge-shaped computational domain

Greek

α	profile shape factor for energy ($= \overline{u^3}/\bar{u}^3$)
β	profile shape factor for momentum ($= \overline{u^2}/\bar{u}^2$)
$\delta x, \delta r$	size of a computational cell
μ	dynamic viscosity
ρ	density
σ	area ratio
τ	shear stress

Subscripts

c-th	theoretical values corrected for friction and momentum effects
cc-th	theoretical values corrected for friction, momentum, and pressure effects
F	fully-developed wall frictional contribution
I	irreversible contribution
inl	inlet conditions
num	numerical value
$p0$	nonuniform pressure effect
R	reversible contribution
RI	total coefficient of pressure without fully developed friction contribution ($R + I$)
T	total pressure coefficient
th	standard theoretical value
r	radial direction
x	axial direction
w	pipe wall
β	momentum effect
01	plane just upstream of the expansion
02	plane just downstream of expansion
1	inlet pipe
2	outlet pipe

Superscripts

′	denotes actual value of wall friction
−(overbar)	cross-section area average
=(double overbar)	straight line fit
~ (tilde)	modified pressure coefficient

pressure drop results are preceded by an assessment of the uncertainties of the calculations and by comparisons of other computed quantities with experimental data and correlations to validate the procedures. This paper ends with a summary of the main conclusions.

Theory

As mentioned above, we concentrate on the laminar flow in a pipe expansion with a fully developed condition some distance upstream of the sudden expansion plane. For reasons that become evident later, the fully developed condition is not applied at the inlet section proper; rather there is a long pipe upstream of the expansion, and the flow is allowed by develop from a rectangular inlet profile to a fully developed flow, well before reaching the sudden expansion plane. The following theoretical derivation is based on the nomenclature and geometry of Figure 1.

In pressure drop calculations in piping networks, it is engineering practice to consider that the flow is fully developed in the straight pipes or ducts, with all other effects, such as flow distortions and redevelopment in fittings, curves, and other elements, introduced via their respective local loss coefficients. Therefore, the total pressure variation between stations 1 and 2 of the sudden expansion (see Figure 1) is usually decomposed into a reversible pressure increase (Δp_R-Bernoulli effect attributable to the decrease of velocity across the expansion), an irreversible pressure drop (Δp_I), which includes the inefficient dissipation of kinetic energy as the fluid decelerates, thus creating a recirculation zone, and the pressure variation attributable to *fully developed friction* on the walls (Δp_F):

$$\Delta_{p_T} \equiv p_2 - p_1 = \Delta p_R - \Delta p_I - \Delta p_F \tag{1}$$

In this way, the local loss coefficient is identified with the irreversible pressure drop, defined as

$$C_I \equiv \frac{\Delta p_I}{\frac{1}{2}\rho\overline{u_1}^2} \tag{2}$$

Clearly, C_I includes a friction effect, because the actual friction between stations 1 and 2 (this is denoted $\Delta p'_F$) is certainly different from the corresponding fully developed friction. The terms in Equation 1 can be written as pressure difference coefficients, based on the *upstream* dynamic pressure, as defined in Equation 2 unless otherwise stated, so that it becomes

$$C_T = C_R - C_I - C_F \equiv C_{RI} - C_F \tag{3}$$

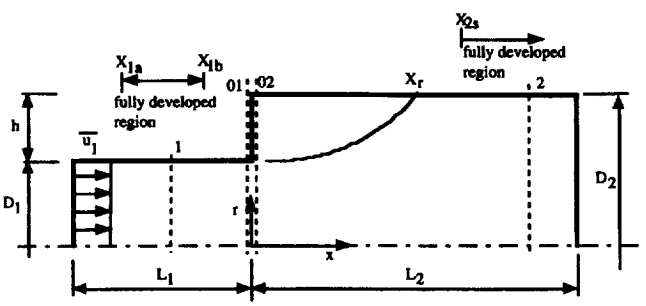

Figure 1 The sudden expansion geometry and its control volume

In the derivation below it will be necessary to introduce the profile shape factors for energy, $\alpha = \overline{u^3}/\overline{u}^3$ and momentum $\beta = \overline{u^2}/\overline{u}^2$, where an overbar denotes area averaging. Integral conservation of momentum and energy applied to the control surface formed by stations 1 and 2, where the flow is assumed to be fully developed, and the inside pipe walls, is expressed as:

$$p_1 A_1 + \rho A_1 \beta_1 \overline{u_1}^2 + (A_2 - A_1)\bar{p}_{02} = p_2 A_2 + \rho A_2 \beta_2 \overline{u_2}^2 + A_1 \Delta p'_{F1} + A_2 \Delta p'_{F2} \tag{4}$$

$$p_1 + \tfrac{1}{2}\rho\alpha_1\overline{u_1}^2 = p_2 + \tfrac{1}{2}\rho\alpha_2\overline{u_2}^2 + \Delta p_{F1} + \Delta p_{F2} + \Delta p_I \tag{5}$$

The fully developed friction terms of Equation 5 are given by

$$\Delta p_{F1} = f_1 \frac{L_1}{D_1}\frac{1}{2}\rho\overline{u_1}^2 \tag{6a}$$

$$\Delta p_{F2} = f_2 \frac{L_2}{D_2}\frac{1}{2}\rho\overline{u_2}^2 \tag{6b}$$

In Equation 4, the pressure $\bar{p}_{02}$ is an area-average pressure acting on the step wall area $A_2 - A_1$, just downstream of the expansion. At stations 1 and 2 the pressure is assumed uniform, and, therefore the overbar is unnecessary. The symbol $\Delta p'_F$ represents the actual integrated wall stress calculated by

$$\Delta p_F \equiv \frac{1}{A}\int_a \tau_w \, da = \frac{1}{(\pi D^2/4)}\int_L \tau_w \pi D \, dx = \frac{4}{D}\int_L \tau_w \, dw = 4\frac{L}{D}\bar{\tau}_w \tag{7}$$

where A is the cross-sectional area and a the wetted perimeter area.

In a reversible flow, the energy equation reduces to the Bernoulli equation:

$$p_{1R} + \frac{1}{2}\rho\alpha_1\overline{u_1}^2 = p_{2R} + \frac{1}{2}\rho\alpha_2\overline{u_2}^2 \Rightarrow \Delta p_R \equiv (p_2 - p_1)_R = \frac{1}{2}\rho\alpha_1\overline{u_1}^2\left[1 - \frac{\alpha_2}{\alpha_1}\left(\frac{\overline{u_2}^2}{\overline{u_1}^2}\right)\right] \tag{8}$$

From mass conservation $A_1\overline{u_1} = A_2\overline{u_2}$ and after defining the area ratio as $\sigma = A_1/A_2$, the reversible pressure increase coefficient becomes

$$C_R = \alpha_1\left(1 - \frac{\alpha_2}{\alpha_1}\sigma^2\right) \tag{9}$$

Some manipulation of Equation 4 yields

$$C_T \equiv \frac{p_2 - p_1}{\frac{1}{2}\rho\overline{u_1}^2} = 2\beta_1\sigma\left(1 - \frac{\beta_2}{\beta_1}\sigma\right) - \left[\frac{\Delta p'_{F2} + \sigma\Delta p'_{F1} - (1-\sigma)(\bar{p}_{02} - p_1)}{\frac{1}{2}\rho\overline{u_1}^2}\right] \tag{10}$$

To eliminate pressure p_1 from this equation, it is necessary to perform again a momentum balance, this time to the control volume between stations 1 and 01 (Figure 1):

$$p_1 A_1 + \rho A_1 \beta_1 \overline{u_1}^2 = \bar{p}_{01} A_1 + \rho A_1 \beta_{01} \overline{u_1}^2 + A_1 \Delta p'_{F1} \tag{11}$$

where β_{01} is the momentum factor just upstream of the expansion. Introducing this equation into the one above, yields:

$$C_T = 2\beta_1 \sigma \left(1 - \frac{\beta_2}{\beta_1}\sigma\right) - \left[C'_{F2} + C'_{F1} - 2(1-\sigma)(\beta_1 - \beta_{01}) + (1-\sigma)\left(\overline{C}_{p01} - \overline{C}_{p02}\right)\right] \tag{12}$$

where the actual friction coefficients are denoted by a prime. The area-averaged pressure coefficients at the expansion plane in Equation 12 follow from the adopted notation:

$$\overline{C}_{p01} \equiv \frac{\overline{p_{01}}}{\frac{1}{2}\rho \overline{u_1}^2} = \frac{1}{\frac{1}{2}\rho \overline{u_1}^2 A_1} \int_{A_1} p_{01}\, \mathrm{d}A \tag{13a}$$

$$\overline{C}_{p02} \equiv \frac{\overline{p_{02}}}{\frac{1}{2}\rho \overline{u_1}^2} = \frac{1}{\frac{1}{2}\rho \overline{u_1}^2 A_0} \int_{A_0} p_{02}\, \mathrm{d}A \qquad (\text{with } A_0 = A_2 - A_1) \tag{13b}$$

Similarly, for the fully developed and the actual wall friction coefficients, respectively,

$$C_{F1} \equiv \frac{\Delta p_{F1}}{\frac{1}{2}\rho \overline{u_1}^2} = f_1 \frac{L_1}{D_1}, \qquad C'_{F1} \equiv \frac{\Delta p'_{F1}}{\frac{1}{2}\rho \overline{u_1}^2} = 4\frac{L_1}{D_1}\frac{\overline{\tau_{w1}}}{\overline{u_1}^2} \tag{14a}$$

in the inlet pipe, and

$$C_{F2} \equiv \frac{\Delta p_{F2}}{\frac{1}{2}\rho \overline{u_1}^2} = \sigma^2 f_2 \frac{L_2}{D_2}, \qquad C'_{F2} \equiv \frac{\Delta p'_{F2}}{\frac{1}{2}\rho \overline{u_1}^2} = 4\frac{L_2}{D_2}\frac{\overline{\tau_{w2}}}{\frac{1}{2}\rho \overline{u_1}^2} \tag{14b}$$

in the outlet pipe. The irreversible loss coefficient is now obtained from the decomposition defined by Equation 3; i.e.,

$$C_I = \alpha_1\left(1 - \frac{\alpha_2}{\alpha_1}\sigma^2\right) - 2\beta_1\sigma\left(1 - \frac{\beta_2}{\beta_1}\sigma\right) - \left[\Delta C_F + 2(1-\sigma)(\beta_1 - \beta_{01}) - (1-\sigma)\left(\overline{C}_{p01} - \overline{C}_{p02}\right)\right] \tag{15}$$

where the following definitions were introduced

$$\Delta C_F \equiv C_F - C'_F$$

with

$$\Delta C_{F2} \equiv (C_{F2} - C'_{F2}) \qquad \text{and} \qquad \Delta C_{F1} \equiv (C_{F1} - C'_{F1}) \tag{16}$$

which represent the difference between fully developed pressure drop and the actual pressure drop due to a variable wall shear stress. Equation 15 is the main result of this analysis and may be written in a compact notation as:

$$C_I = (C_I)_{\text{th}} - \{\Delta C_F + \Delta C_\beta - \Delta C_{p0}\} \tag{17}$$

where $(C_I)_{\text{th}}$ is the standard theoretical loss coefficient (two first terms on the right-hand side of Equation 15) and the corrective factors other than those due to wall friction are defined as:

$$\Delta C_\beta \equiv 2(1-\sigma)(\beta_1 - \beta_{01}) \tag{18}$$

and

$$\Delta C_{p0} \equiv (1-\sigma)\left(\overline{C}_{p01} - \overline{C}_{p02}\right) \tag{19}$$

The total pressure variation coefficient, without considering fully-developed wall friction, is given by:

$$C_{RI} = 2\beta_1\sigma\left(1 - \frac{\beta_2}{\beta_1}\sigma\right) + \{\Delta C_F + \Delta C_\beta - \Delta C_{p0}\} \tag{20}$$

Equations 17 and 20 given the correct theoretical values of the irreversible and total (without fully developed fraction) pressure coefficients, respectively. It should be noted that these coefficients do not depend upon the extension of the control volume, provided the flow conditions at the inlet and outlet planes are fully developed, because each pressure difference of type $\Delta p_F - \Delta p'_F$ then tends to a constant value.

The terms in braces in Equations 17 and 20, represent corrections to the standard theory. Whenever the wall friction can be neglected relative to other effects, the momentum and energy coefficients assumed constant along the two pipes, and a uniform pressure is assumed to apply at the expansion plane, then the above equations reduce to the following "uncorrected," but widely used formulas here referred to as the standard theory: $(C_I)_{\text{th}} = (1-\sigma)(\alpha + \sigma(\alpha - 2\beta))$; $(C_{RI})_{\text{th}} = 2\beta\sigma(1-\sigma)$. For uniform velocity profiles, then $\alpha = \beta = 1$ and the pressure coefficients become $C_R = (1-\sigma^2)$; $(C_{RI})_{\text{th}} = 2\sigma(1-\sigma)$; $(C_I)_{\text{th}} = (1-\sigma)^2$, which are the equations usually found in textbooks and valid to a good approximation for turbulent flows; here $(C_I)_{\text{th}}$ is the so-called Borda–Carnot coefficient. Because the present application is for laminar flow, where the fully developed velocity profile is given by a parabolic law, α and β take the values 2 and 4/3, respectively. With these values, the "uncorrected" forms of the pressure coefficients become:

$$C_R = 2(1-\sigma^2); (C_{RI})_{\text{th}} = \tfrac{8}{3}\sigma(1-\sigma); (C_I)_{\text{th}} = 2(1-\sigma)(1-\tfrac{1}{3}\sigma) \tag{21}$$

In the pressure variation Section 4, it is shown that the corrective terms within the braces of Equations 17 and 20 are important. Because these corrections cannot be evaluated theoretically, they either have to be computed from numerical results or experimentally measured. The former was the option for this work, and planes 1 and 2 were selected in regions of fully developed flow, as mentioned above; i.e., the energy and momentum factors are $\alpha_1 = \alpha_2 = 2$ and $\beta_1 = \beta_2 = 4/3$, respectively.

Calculation procedure

In this section, the numerical method adopted for solution of the transport equations is fully described and details are given on the grid testing. After selection of an adequate grid, the programme is further validated by carrying out a number of comparisons with experimental and numerical data from the literature. In this section, the focus is on such quantities as the recirculation length and eddy intensity, and the prediction of the pressure variation for the fully developed pipe flow regions.

Numerical method and grid testing

The mass and momentum differential conservation equations were discretised by the control volume-based finite difference scheme described by Patankar (1980), and later adapted by Perić (1985) for nonstaggered, nonorthogonal grids. The main code is interfaced with a mesh generation preprocessor and adequate data post processor, as described by Oliveira (1992). The basic differencing schemes were all second order; namely, central differencing for the diffusion terms and the linear upwind scheme (LUDS), described by Perić, for the convective terms. The pressure velocity coupling was dealt with by a time-marching form of the SIMPLEC algorithm and all the calculations were performed in a HP 715/75 workstation.

Solution of the present two-dimensional (2-D) axisymmetric flow with a full three-dimensional (3-D) code based on Cartesian velocity components requires use of a computational domain with the shape of a wedge of triangular cross section. This entails a small difference (less than 1.2%) between the actual and the computational cross-sectional area; in the comparison with the theory, the average velocity is corrected as $(A\bar{u})_{th} = (A\bar{u})_{num}$, to maintain the flow rate, with $A_{th} = (\pi D^2/4)\ (15/360)$ for a section having a 15° angle at the apex and $A_{num} = YZ$. Results presented in the pressure variation section (namely, the radial profiles of the fully developed axial velocity component in Figure 6 and the differences of no more than 0.4% and 0.7% between the predicted and theoretical friction factors in the inlet and outlet fully developed pipe flows, respectively) prove that this small correction does not introduced any artefacts into the analysis.

The boundary conditions were as follows. On the two side planes of the wedge symmetry, boundary conditions were set; on the centreline, the boundary condition was axisymmetry; and at the wall, all velocity components were set to zero. In the outflow plane, the longitudinal velocity gradients for all components of the velocity vector were also set to zero. This outflow plane was located far downstream of the expansion to allow a complete flow redevelopment. At the inlet duct, the flow was allowed to develop from a plug velocity profile into the traditional parabolic shape well before reaching the expansion plane. The ratio of the inlet pipe (D_1) to the outlet pipe (D_2) diameters defined the expansion ratio used throughout this paper.

The computational grids were generated using patched blocks, one for the inlet pipe and two for the larger outlet pipe. The presence of the inlet pipe does not create any numerical difficulty (such as computational cells out of the flow domain) because of use of a special indirect addressing strategy, as explained in Oliveira (1992). Except in some initial testing, the mesh spacing was nonuniform, with more mesh points concentrated near the expansion plane and along the wall of the inlet pipe, so as to properly resolve the shear layer starting at the expansion corner. Also, for purposes of mesh continuity, the expansion factors used to define the control volume dimensions were carefully chosen to guarantee a smooth variation in the whole domain, with particular attention to the interface between the mesh-generating blocks. Finally, following the recommendations of Castro (1979), the local cell Reynolds number in the vicinity of the corner did not exceed, and was usually considerably lower than, a value of about 1.0, in order to reduce possible errors generated at the corner, which may then be convected downstream.

A series of tests with different grids was initially performed to assess the adequate size of the computational domain for grid-independent results and to help define the length of the inlet and outlet ducts required for full velocity profile development. In this preliminary stage of the investigation, the effect of much refinement and the relationship between all those parameters, the Reynolds number, and the accuracy of the results were analysed.

The grid analysis closely followed the 1:2.6 sudden expansion of Back and Roshke's (1972) experiments. A uniform velocity profile was assigned at the inlet of a short duct (here taken as $L_1 = D_1$), located upstream of the sudden expansion, defining an inlet Reynolds number equal to 50. Table 2 gives some characteristics of the computational meshes and the corresponding predicted recirculation bubble length. Grid 3 has the double number of cells along x, in the outlet pipe, compared with grid $2n$, and the number of cells along r was then doubled for grid 4. More details of the mesh refinement study can be found in Oliveira and Pinho (1995).

The results of Table 2 indicate that further grid refinement beyond that of grid $2n$ does not improve the prediction of x_r and that the uncertainty of the results is, at most, 0.2%. Similar conclusions were drawn from inspection of the predicted pressure profiles and maximum values of the stream function within the recirculation zone. The key factor is the smallest mesh spacing in the vicinity of the re-entrant corner. The uncertainty remains constant with the Reynolds number, provided the minimum spacing in both the x- and r-directions in that region is about 0.10 mm (in nondimensional form $\delta x/(D_1/2) \approx 1/47$ and $\delta x/((D_2 - D_1)/2) \approx 1/76$). For the higher-Reynolds number flows, the domain had to be extended further on the downstream side of the expansion, in order to attain fully developed flow, but always maintaining the main geometric characteristics of the grid $2n$ as in Table 2. Other characteristics of this grid for the Back and Roshke's runs were: $NX = 20$ and $NR = 20$ with $f_x = 0.874$ and $f_r = 0.924$ for the inlet pipe block; $NX = 70$ and $NR = 20$ with $f_x = 1.091$ and $f_r = 0.924$ for the outlet pipe block downstream of the inlet pipe; and $NX = 70$ and $NR = 32$ with $f_x = 1.091$ and $f_r = 1.05$ for the outlet pipe block located downstream of the expansion wall.

Validation tests

In this validation, the experimental results of the 1:2.6 expansion of Back and Roshke (1972), already used in the grid tests, and the 1:2 expansions of Marcagno and Hung (1967) and Halmos and Boger (1975) were selected. The experimental results of the latter authors were also accurately predicted by the numerical computations of Halmos *et al.* (1975).

The numerical correlations developed by Scott *et al.* (1986), specifically for the 1:2 sudden expansion, and the more general correlations of Badekas and Knight (1992), which are valid for a

Table 2 Maximum and minimum grid size and predicted recirculation length (Re = 50)

Grid	NC	δx_{min}	δr_{min}	δx_{max}	δr_{max}	x_r
Grid 1	4040	0.24	0.24	34.7	0.24	35.5
Grid 2	4040	0.24	0.10	34.7	0.45	35.7
Grid 2n	4040	0.10	0.10	41.4	0.45	35.6
Grid 3	7680	0.10	0.10	18.3	0.45	35.6
Grid 4	13760	0.10	0.10	18.3	0.14	35.6

NC = total number of internal cells for $L_1 = D_1$, values in mm; note that $D_1 = 0.5$ mm

wider range of expansion ratios, were also used here. Whereas the numerical correlations derived by Scott *et al.* (1986) for various quantities are optimised for each particular expansion ratio, those of Badekas and Knight are general and are based on a compilation of data from different sources of both computational and experimental work; thus, they are prone to a higher uncertainty. The latter authors also indicate that their correlations are only valid for inlet Reynolds numbers between 50 and 200.

Prediction of the recirculation length of Back and Roshke's (1972) flow, with a plug velocity profile imposed one diameter upstream of the plane of the expansion, did not compare well with the experimental data, as can be seen in Fig. 2a, because of the difficulty in assessing the correct inlet condition used in the experiments. The sudden expansion of Back and Roshke's experiments was located immediately downstream of the settling chamber with a very short inlet pipe between the two. So, the real velocity profile at the exit of the settling chamber was never a plug flow because of the no-slip condition at the wall.

Using a longer inlet duct, with a fully developed velocity profile, yielded results much closer to the measurements of Back and Roshke (1972). To achieve the fully developed inlet profile, a uniform velocity profile was submitted to a long inlet section of $L_1/D_1 = 20$, as shown in Figure 1. Note that the higher Reynolds number investigated here was less than 250, for which the Langhaar formula (White 1979) predicts a development length of $L_1/D_1 = 0.0575\ \mathrm{Re} = 14.4$. The differences in the predictions show how important it is to compare data pertaining to well-defined inlet conditions, because the flow characteristics downstream of the expansion are strongly sensitive to it, and especially so to the velocity in the wall region of the inlet pipe. To quantify this point, the prediction of X_r with the uniform velocity profile imposed right at the expansion (no inlet section) is 30% shorter than the previous case of $L_1 = D_1$ (for $\mathrm{Re} = 200$). Also, in preliminary studies differences of about 6% were observed in X_r when the fully developed velocity profile is imposed at $x = 0$ compared to the case of naturally developed flow in a long inlet section. Thus, the remaining comparisons with the literature pertain to a well-defined inlet condition, that of a fully developed flow imposed some distance upstream of the sudden expansion. In this case, there is a significant improvement in the predictions, as well as in comparison with the correlation of Badekas and Knight (1992) for a fully developed inlet flow, also included in Figure 2a.

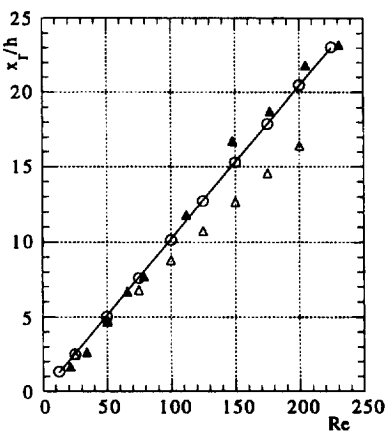

Figure 2a Recirculation bubble length versus inlet Reynolds number for a 1:2.6 sudden expansion flow of Newtonian fluids; ▲ Back and Roschke; ○ long inlet prediction; △ short inlet prediction; — Badekas and Knight (1992)

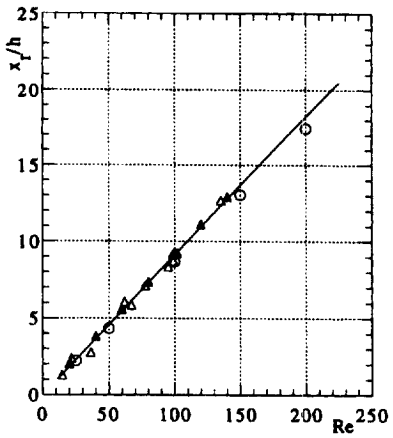

Figure 2b Recirculation bubble length versus inlet Reynolds number for a 1:2 sudden expansion flow of Newtonian fluids; ▲ Halmos *et al.* (1975); — Badekas and Knight (1992); △ Macagno and Hung, ○ prediction

Figure 2b concerns a 1:2 expansion and includes data from Macagno and Hung (1967), the Newtonian predictions of Halmos *et al.* (1975), the correlation of Badekas and Knight (1992) and our numerical predictions. This time, the data are very close to each other, with our predictions and Macagno and Hung's results very slightly lower than the correlation of Badekas and Knight, a good result that now stems from well-known and well-defined inlet velocity profiles. The linear dependence of the recirculation length on the Reynolds number is a well-established result also observed here, provided the Reynolds number is not too small, and it comes as no surprise that the correlation of Badekas and Knight for the 1:2 expansion ratio is the same as that proposed before by Scott *et al.* (1986).

The comparisons between the current predictions and Badekas and Kings (1992) correlation for the relative eddy intensity are in Figure 3, for both expansion ratios. The differences are under 7 and 5% for the expansion ratios of 2 and 2.6, respectively. Nonlinearities in the correlated quantities makes it more difficult to develop universal correlations (as is the case of Badekas and

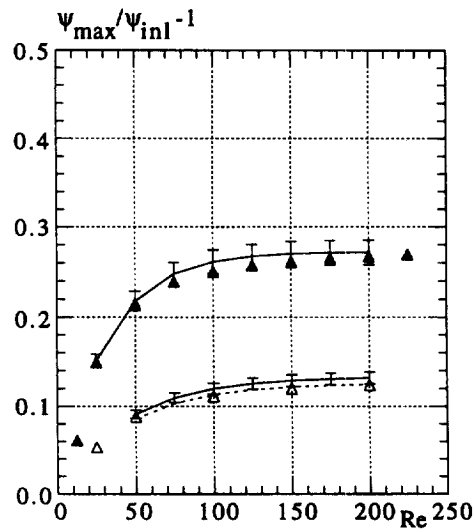

Figure 3 Comparison between calculated (△), Badekas and Knight's (1992) correlation (—) and Scott *et al.* (1986) correlation (----) for the relative eddy intensity, with ±5% error bars; open symbol (1:2); closed symbols (1:2.6)

Knight equation), and this is well shown in the good comparison of our predictions with the specific equation developed by Scott *et al.* (1986) for the 1:2 expansion.

The discrepancies between Badekas and Knight's (1992) general correlation and Scott *et al.*'s (1986) specific correlation are particularly well shown in the comparisons pertaining to the eddy centre location in Figure 4. The determination of the recirculation length relies on the interpolation close to the wall; whereas the eddy centre is the locus of the maximum value of the stream function, which happens in a region of elongated shape. So, the calculation of the maximum value of the stream function is not so accurate as the determination of the eddy length, but despite this, the current predictions are within 2.5% of those of Scott *et al.* for the same expansion ratio. The general correlation of Badekas and Knight behaves better at larger expansion ratios (less than 10% difference) than at smaller expansion ratios, where the discrepancies can be more than 20%. This is also clear from the major difference between the two equations, which have a zero (Badekas and Knight) and a nonzero (Scott *et al.*) ordinate, from which results some different behaviour of the correlations.

The set of extensive comparisons with well-defined cases, together with the grid refinement study of the previous section, was deemed sufficient to validate all aspects of the calculation procedure and to give us confidence in its capacity to predict other such flow characteristics as the pressure variation through the expansion accurately, which is the main objective of this work and for which experimental data are scarce in the Reynolds number range here considered.

Pressure variation: results and discussion

The investigation of the pressure coefficient behavior was undertaken in the 1:2.6 sudden expansion geometry of Back and Roshke (1972), but for the fully developed inlet condition defined well upstream of the expansion plane.

First, the computed fully developed flow friction factors in the upstream and downstream pipes were compared to the theoretical values. The Darcy fraction factors can be computed from their definition

$$\Delta p = f\frac{L}{D}\frac{1}{2}\rho\bar{u}^2 \Rightarrow f = \frac{\Delta(p/\frac{1}{2}\rho\bar{u}^2)}{\Delta(x/D)} \equiv \frac{\Delta C_p}{\Delta X} \tag{22}$$

with the derivative obtained from curve fitting pressure variation along the axis. Instead of directly fitting a straight line to the numerical data of C_p versus $x(r=0)$, it has been found more accurate to use a different pressure function defined as:

$$\tilde{C}_p \equiv \frac{p}{\frac{1}{2}\rho\bar{u}_1^2} \quad \text{for} \quad x \le 0, \quad \text{and}$$

$$\tilde{C}_p \equiv \frac{p}{\frac{1}{2}\rho\bar{u}_2^2} - \frac{(1-\sigma^2)\bar{\bar{C}}_{p01} + C_R}{\sigma^2} \quad \text{for} \quad x > 0 \tag{23}$$

where $\bar{\bar{C}}_{p01}$ is the intercept with the y-axis at $x=0$ of the straight line fitted to the fully developed C_p data pertaining to $x \le 0$.

This modified $\tilde{C}_p$ has the advantage of possessing the same inclination along the smaller and the larger pipes; whereas, the curve of C_p versus x (Figure 5a) flats out along the larger pipe ($x > 0$) impeding an accurate line-fitting from which both f and C_I are determined. The friction factor f results from the inclination of $\tilde{C}_p$, and C_I from the intersection with the y-axis, of the straight line fit given by the equations:

$$\bar{\bar{C}}_p = -f_1 X + \bar{\bar{C}}_{p01} \; (X \le 0) \quad \text{and}$$

$$\bar{\bar{C}} = -\frac{f_2}{D_2/D_1}X + \bar{\bar{C}}_{p02} \; (X > 0) \tag{24}$$

which are represented by the solid lines in Figure 5b, for Re = 200. It is straightforward to check that the local irreversible loss coefficient can then be determined from the difference of values of $\bar{\bar{C}}_p$ at the intersection with the y-axis at $x=0$, thus

$$C_I = \sigma^2\left(\bar{\bar{C}}_{p01} - \bar{\bar{C}}_{p02}\right) \tag{25}$$

An additional precaution to limit the errors inherent to the line-fitting of Equation 24, and their propagation in the evaluation of C_I, is to apply the fitting process only to those points

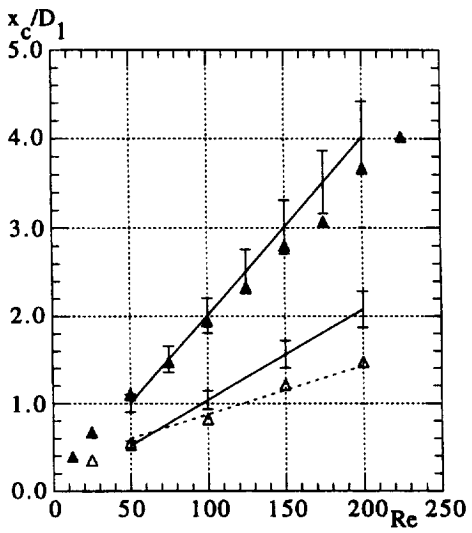

Figure 4 Comparison between calculated (△), Badekas and Knight's (1992) correlation (—) and Scott *et al.* (1986) correlation (----) for the location of the eddy centre, with ±10% error bars; open symbols (1:2); closed symbols (1:2.6)

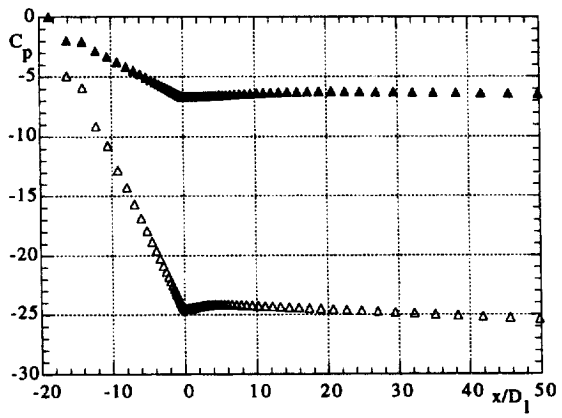

Figure 5a Variation of the pressure coefficient C_p along the pipe axis for the Reynolds numbers of 50 (△) and 200 (▲)

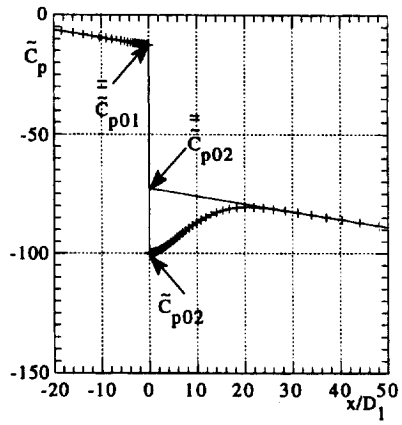

Figure 5b Variation of $\tilde{C}_p$ and straight line fitting in the inlet and outlet pipes ($\bar{\bar{C}}_p$) for Re = 200

lying in the regions of fully developed flow; i.e., for $X_{1a} < X < X_{1b}$ in the small diameter pipe and $X > X_{2s}$ in the larger pipe (see Figure 1). This range was checked for every Reynolds number, typical values being $[X_{1a}, X_{1b}] = [-10, -0.5]$ and $X_{2s} = 15$ but $|X_{1b}|$ tending to increase as Re decreases ($X_{1b} = -1.2$ for Re = 1). Without this precaution, the error committed on C_f was about 2.5% at Re = 100.

Values of the friction factor obtained from Equation 22, following this line-fitting procedure, agreed to within 0.7%, with the theoretical Darcy friction factor for laminar flow, $f_{th} = 64/\mathrm{Re}$. An alternative way is to compute the friction factors from the wall shear stress, as stems from a momentum balance, which for the wedge-shaped cross section, yields

$$f = \frac{4\tau_w}{\frac{1}{2}\rho\bar{u}^2}\frac{D}{2Y} \tag{26}$$

with τ_w calculated from Newton's law of the viscosity

$$\tau_w = \mu(\partial u/\partial r). \tag{27}$$

The corrective term on the right-hand side of Equation 26 takes into account the differences in cross-section shape and is equal to 1.0085 and 1.0090 for the upstream and downstream pipes, respectively. Values of the friction factor obtained with this alternative procedure were virtually identical to those from equation 22, demonstrating the self-consistency of the computed results and giving an additional justification for the corrective factor $D/2Y$ in Equation 26. Were that factor not included, and an apparent imbalance of about 0.9% would have arisen between the pressure drop and the wall stress.

The marks in Figure 5a are the predicted C_p along the axis of symmetry for two flow cases, Re = 50 and 200. If the fully developed linear pressure decay on both sides of the expansion were extrapolated to the expansion plane ($x = 0$), there would result a net pressure increase, the pressure jump at $x = 0$, here denoted $C_{RI} = \bar{\bar{C}}_{p02} - \bar{\bar{C}}_{p01}$. With the reversible pressure rise C_R given by Equation 9, which yields $C_R = 1.956$ for a parabolic velocity profile, then from Equation 3 we would obtain the loss coefficient: $C_f = C_R - C_{RI}$. Instead of that, with the modified pressure coefficient $\tilde{C}_p$, plotted in Figure 5b for Re = 200, the loss coefficient results directly according to Equation 25.

The left part of Table 3 gives the irreversible loss coefficient computed from Equation 25 with the predicted numerical values of C_p, as well as the total pressure coefficient of Equation 3 without the fully developed friction contribution (C_{RI}), for various Reynolds number flows. At low-Reynolds numbers, the local loss coefficient (C_f) is inversely proportional to the Reynolds number, because the flow characteristics of the sudden expansion are dominated by the viscous forces. Here we encounter the typical straight line variation of the loss coefficient with the Reynolds numbers in log–log coordinates, shown later in Figure 9 of this work, a behavior similar to that of fully developed laminar duct flows, where by virtue of symmetry conditions, the convective terms of the Navier–Stokes equation vanish.

However, at high-Reynolds numbers, the flow downstream of the expansion becomes dominated by inertial forces, and the local loss coefficient tends to a constant value. Here C_{RI} is positive, thus indicating that the reversible pressure increase (C_R) is greater than the irreversible pressure drop (C_f), but for low-Reynolds numbers, this trend is reversed to that close to Re = 1, the coefficient C_f is one order of magnitude higher than C_R and increasing for lower values of the Reynolds number. The uncorrected theoretical values of the irreversible and C_{RI} coeffi-

Table 3 Predicted (C_f), corrections, and corrected theoretical ($C_{fc\text{-}th}$) loss coefficients at the expansion

Re	C_f	C_{RI}	x_r/D_1	β_{01}	ΔC_β	ΔC_{F1}	ΔC_{F2}	$C_{fc\text{-}th}$	error %
1	16.61	−14.65	0.41	1.223	0.188	−2.588	1.225	2.800	+494
2	8.369	−6.413	0.45	1.228	0.180	−1.250	0.644	2.046	+309
3.5	4.830	−2.874	0.52	1.237	0.164	−0.678	0.402	1.732	+178
5	3.458	−1.502	0.59	1.244	0.152	−0.453	0.310	1.611	+114
10	1.981	−0.025	0.89	1.265	0.116	−0.200	0.226	1.476	+34
12.5	1.726	0.230	1.06	1.272	0.105	−0.111	0.217	1.410	+22
17.5	1.508	0.448	1.43	1.282	0.0875	−0.0992	0.218	1.414	+6.6
25	1.379	0.577	2.01	1.292	0.0704	−0.0468	0.227	1.370	+0.8
35	1.331	0.625	2.81	1.299	0.0585	−0.0404	0.237	1.365	−2.5
50	1.306	0.650	4.03	1.306	0.0466	−0.0189	0.247	1.346	−2.9
75	1.301	0.655	6.07	1.312	0.0364	−0.0110	0.256	1.339	−2.8
100	1.304	0.652	8.13	1.316	0.0295	−0.0074	0.261	1.337	−2.5
125	1.308	0.648	10.18	1.319	0.0244	−0.0055	0.262	1.337	−2.2
150	1.311	0.645	12.24	1.320	0.0227	−0.0043	0.266	1.336	−1.9
175	1.312	0.644	14.32	1.322	0.0193	−0.0045	0.267	1.338	−1.9
200	1.315	0.641	16.39	1.323	0.0176	−0.0037	0.269	1.338	−1.7
225	1.317	0.639	18.45	1.324	0.0159	−0.0032	0.270	1.338	−1.6

Note: $C_R = 1.956$

cients, given by Equation 21 of the standard theory yield $(C_I)_{th} = 1.620$ and $(C_{RI})_{th} = 0.336$, which may be compared with the computed values in Table 3. There is considerable difference and; whereas the standard theory yields independent of the Reynolds number, the predictions do show a variation, which is very intense at low-Reynolds numbers and of the order of 20 and 50% at high-Reynolds numbers for C_I and C_{RI}, respectively. To explain this discrepancy, the uncorrected standard theory coefficients were corrected with the first two terms within the braces of Equation 17, which were evaluated from the numerical results and are also given in Table 3. This table does not include the effect of nonuniform pressure at the expansion plane, the last of the three terms within the braces, which will be considered later.

On the right part of Table 3, β_{01} is the momentum factor at the expansion, computed from the numerical integration of the velocity profile just upstream of the expansion plane, and the corrective coefficient ΔC_β is the term defined in Equation 18. The presence of the expansion distorts the velocity profile from its parabolic shape just upstream of the expansion plane, making β_{01} depend on the Reynolds number and differ from the theoretical value of $4/3 \approx 1.333$. The difference entails a corrective factor ΔC_β to be subtracted from the theoretical C_I, which is quite important for the low-Reynolds number flows and drops to about 1.5% at higher-Reynolds numbers.

The upstream influence of the expansion was assessed from plots of the streamlines and pressure contours. These are not presented here for brevity, but the main resulting points pertaining to typical low- and high-Reynolds number cases are briefly discussed. The pressure field at the entrance was much more distorted for Re = 12.5 than for Re = 200. At low-Reynolds numbers, the influence of inertial forces is small compared with that of molecular diffusion, which acts in all directions and clearly influences the flow upstream via two effects. First, there is a stronger radial viscous diffusion of momentum, which changes the shape of the recirculation bubble, as indicated in the different curvature of the streamlines. Whereas the separation streamline for Re = 200 follows the direction of the oncoming flow and starts to curve further downstream (convex bubble shape) behaving like a mixing layer between a jet and the recirculating region, the separation streamline for Re = 12.5 curves immediately at the expansion edge (concave bubble shape). The second effect stems from the axial viscous diffusion, which gives the flow some predictive memory; it will sense the oncoming expansion and the flow starts to change earlier than for the higher-Reynolds number inertia-dominated flow.

The velocity profile distortion is shown in the comparison between the radial profiles of the axial velocity component some distance upstream from the expansion, and just before the expansion (station 01) in Figure 6, for Reynolds numbers of 12.5 and 100. The velocity profile attains a fully developed parabolic shape for $X < -1$, but it is then distorted by the presence of the expansion and deviates "considerably" from that shape at the entrance of the expansion. This deviation is more pronounced for the low-Reynolds number case (Re = 12.5), for which α_{01} also changes to 1.810 (instead of the fully developed parabolic profile value of 2) and β_{01} becomes 1.272 (instead of 1.333), as would be anticipated from the increased pressure distortion to be discussed below. For Reynolds numbers below 12.5, these effects are intensified, thus explaining the higher corrections.

The correction resulting from differing actual and fully developed wall friction is quite important for the full range of Reynolds numbers, affecting C_I to a level of about 15 to 20% for Reynolds numbers higher than 50 and increasing in absolute values as the Reynolds number is reduced. The effect is well illustrated in Figure 7, where the actual local friction factor f is compared with the fully developed value (marked f_{th} in the figure). It is also clear from the figure that ΔC_{F1} is negligible for a Reynolds

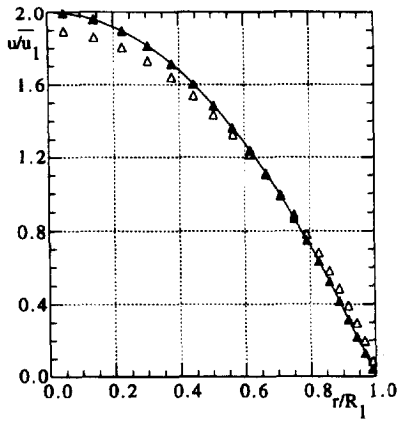

Figure 6a Distortion of the parabolic shape of the velocity profile at the entrance of the expansion (△) relative to the theoretical shape (—) and to the profile at $x/D_1 = -1.2$ (▲) for Re = 12.5

number of around 200, because the flow has a strong convection that maintains the upstream flow fully developed until very close to the expansion. At high-Reynolds numbers, the main contribution to this correction comes from the outlet pipe (ΔC_{F2}) for the same reason; i.e., the strong jet at the expansion takes longer to diffuse to the wall and to evolve towards a fully developed flow.

At lower-Reynolds numbers (less than 10), the correction from the inlet pipe also is important and in such way that it becomes higher (but of the same order of magnitude) than that introduced by the downstream pipe, for two reasons. First, for low-Reynolds number flows, the fully developed friction factor increases and any distortion imposed by the expansion on the upstream pipe, however small, will have a greater impact. Secondly, as the flow slows down with the reduction in the Reynolds number, the longitudinal viscous diffusion becomes more important and contributes more to distort the flow upstream of the expansion, as confirmed by the raising ratio $\Delta C_{F1}/f_1$ and the increased values of ΔC_β.

Initially, it was assumed that the last corrective term within the braces of Equation 17 was of minor importance. However, in order to explain the large discrepancy still present in Table 3 for the low-Reynolds number flows, and also the fact that the error for the higher-Reynolds number flows seems to be systematic, we

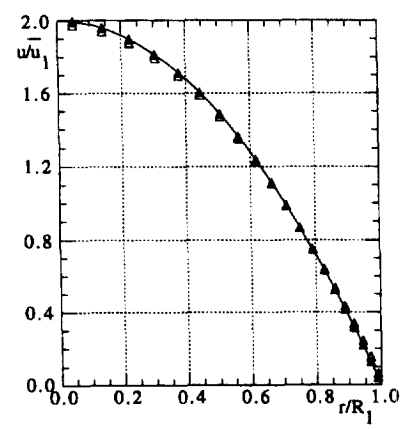

Figure 6b Distortion of the parabolic shape of the velocity profile at the entrance of the expansion (△) relative to the theoretical shape (—) and to the profile at $x/D_1 = -1.2$ (▲) for Re = 100

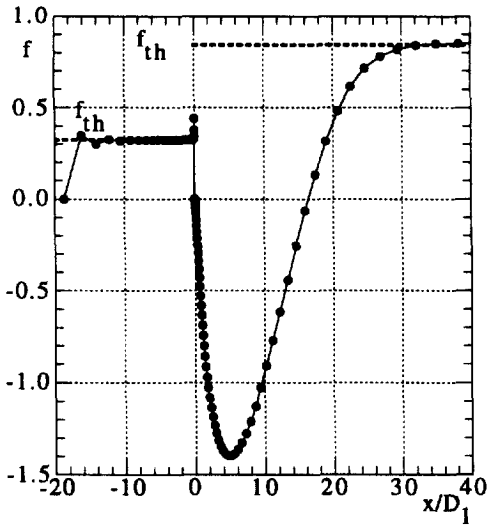

Figure 7 Predicted variation of the friction factor obtained from Equation 26 and 27 and comparison with theory for Re = 200

Table 4 Correction to C_f attributed to nonuniform pressure at the expansion

Re	C_f	ΔC_{p0}	$C_{fc\text{-}th}$	$C_{fcc\text{-}th}$	Error %
1	16.61	14.514	2.80	17.31	4.1
2	8.369	6.645	2.046	8.691	3.7
3.5	4.830	3.290	1.732	5.022	3.8
5	3.458	1.976	1.611	3.587	3.6
10	1.981	0.564	1.476	2.039	2.9
12.5	1.726	0.336	1.410	1.746	1.0
17.5	1.508	0.129	1.414	1.543	2.0
25	1.379	0.025	1.370	1.379	1.0
35	1.331	−0.019	1.365	1.346	1.0
50	1.306	−0.035	1.346	1.311	0.4
75	1.301	−0.036	1.339	1.303	0.1
100	1.304	−0.033	1.337	1.304	0
125	1.308	−0.029	1.337	1.308	0
150	1.311	−0.026	1.336	1.310	0.1
175	1.312	−0.023	1.338	1.314	0.2
200	1.315	−0.021	1.338	1.316	0.1
225	1.317	−0.019	1.338	1.318	0.3

($C_{fc\text{-}th}$ from Table 3 and $C_{fcc\text{-}th}$ is the C_f corrected for all effects)

need to include that effect. The remaining corrective term is attributable to a nonuniform pressure distribution at the expansion plane (the ΔC_{p0} term in Equation 17) observed in the pressure contour plots not presented here but discussed above. The two pressure coefficients in Equation 19 were obtained from area-averaging the numerical results for the pressure distribution immediately upstream (p_{01}) and downstream (p_{02}) of the expansion plane (Figure 1), following exactly the definitions in Equations 13. Because the local pressure profile is not uniform, as shown in Figure 8, $\overline{C}_{p01}$ becomes different from $\overline{C}_{p02}$. In this figure, the y-scale is the same for the two flow cases (Re = 12.5 and Re = 100) in order to emphasise the stronger effect for low-Reynolds numbers.

The final corrected values of the standard theoretical C_f, now including the effects of nonuniform pressure and wall friction, are listed in Table 4. Its inspection shows that the effect of nonuniform pressure at the expansion plane leads to corrections (ΔC_{p0}) of similar magnitude as those arising from upstream velocity profile distortion (ΔC_β in Table 3) for Reynolds numbers higher than 50, but then as the flow tends to the creeping flow regime, it becomes the most important corrective term followed by ΔC_{F1}. Thus, ΔC_{p0} accounts for a difference in C_f of 19% for Re = 12.5, about 1.5% for Re = 225 but increases to more than 85% at Re = 1. In all cases, the application of this correction to the standard theory loss coefficient, following Equation 17, brings the corrected values very close to the predicted values, with differences of less than 0.5% for Reynolds numbers higher than 50 and of less than 4% for the Reynolds number range limited by 1 and 25.

To summarise the work, Figure 9a shows a plot of the local loss coefficient (C_f) as a function of the Reynolds number, as well as its major contributions, as indicated by Equation 17. Inspection of this figure substantiates what has been mentioned

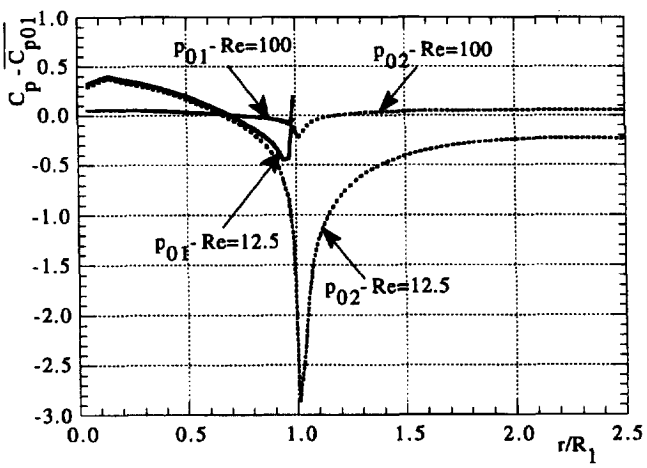

Figure 8 Nonuniformity of the radial pressure profile at the expansion plane: 01—just upstream of the sudden expansion; 02—just downstream of the sudden expansion; pressure coefficients are relative to area-averaged value at station 01

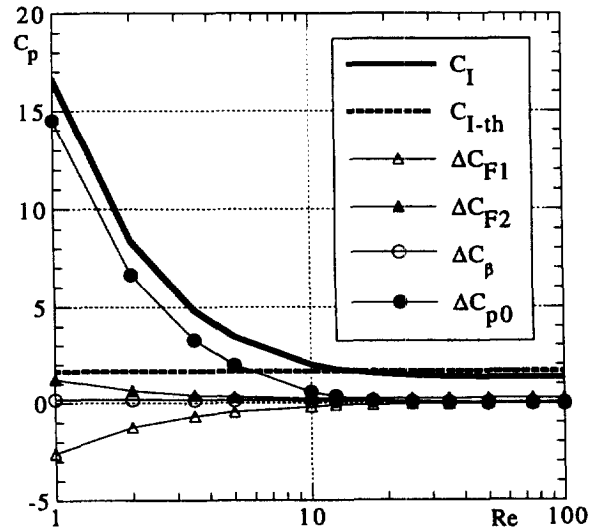

Figure 9a Variation of the local loss coefficient and its contributions with the Reynolds number, for a 1:2.6 sudden expansion

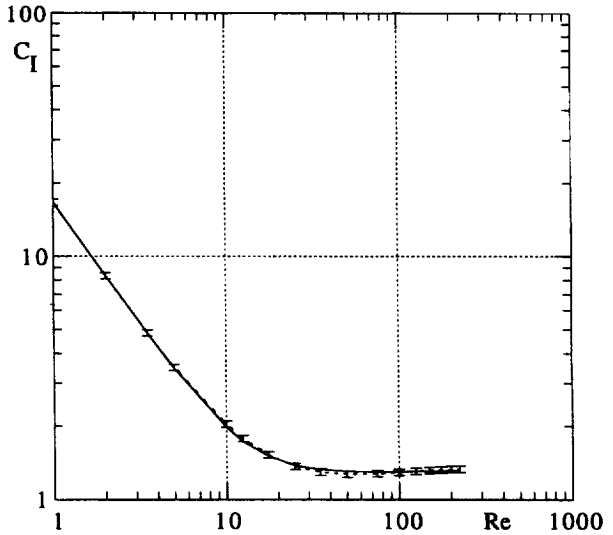

Figure 9b Comparison between the calculated local loss coefficient (full line) and the fitted correlation (Equation 28) with ±3% error bars, for a 1:2.6 sudden expansion

before: ΔC_{p0} is the main contribution to C_I at low-Reynolds numbers and the correction ΔC_{F2} to $C_{I\text{-th}}$ dominates at higher-Reynolds numbers. The low- and high-Reynolds number range can be separated at Re ≈ 17.5. Particularly insightful is the plot of C_I *versus* Re in the log–log scale shown in Figure 9b, from which it is clear that it has two limiting behaviors at low ($C_I = A/\mathrm{Re}$) and high-Reynolds numbers ($C_I = B$), respectively, but the intermediate variation is rather complicated as the value of C_I goes through a minimum. This last effect is brought by the ΔC_{F2} contribution and becomes stronger for larger expansion ratios.

An outcome of the present work with practical importance is the development of a correlation for calculating the local loss coefficient as a function of the Reynolds number and expansion ratio. For the 1:2.6 sudden expansion, with a fully developed inlet flow and Reynolds numbers between 1 and 225, Equation 28 is able to predict the computed local loss coefficient with an accuracy better than 1% Reynolds numbers below 10 and above 50, and an error of 3% in the intermediate range, as shown in Figure 9b.

$$C_I = \frac{19.2}{\mathrm{Re}^{0.93}} - 2.55 + 2.87 \log \mathrm{Re} - 0.542 (\log \mathrm{Re})^2 \qquad (28)$$

The first term on the right-hand side mainly accounts for the viscous behavior, and its form is almost inverse linear as explained throughout the text, and the remaining terms are related to the intermediate and high-Reynolds number behaviour.

The different dependencies of the various corrective terms in Equation 17 on the Reynolds number and expansion ratio, lead to a rather complex correlation for C_I, especially if intended for accurate predictions over a wide range of Reynolds numbers and expansion ratios. The dependence of C_I on the expansion ratio follows $(1 - \sigma)$ for low Re, because, in accordance with Equation 19, $C_I \approx (C_I)_{\mathrm{th}} + \Delta C_{p0}$. For high-Reynolds numbers, $C_I \approx (C_I)_{\mathrm{th}} - \Delta C_{F2}$ and so we would expect to observe $C_I \sigma^{0.5}$ to provide a universal correlation, but an exponent of sigma closer to 0.4 seems more appropriate, although it still fails to provide the correct dependence. The relevance of the many corrective terms at intermediate Reynolds numbers and the way they variate with Re makes C_I go through a minimum and complicates the task of deriving a general equation. Such work is currently under way, and its results will be the subject of a technical note to be presented in the near future, which will include correlations for each corrective term in equation 17 as well as for the total local loss coefficient.

Conclusions

The formulae presented in the literature for calculating the local loss coefficient in sudden expansions is based on the simplified theory that yields values significantly in error for laminar flow, especially at low-Reynolds numbers. To understand those differences and derive better correlations, the quasi-one-dimensional theory for the pressure drop in expansion flows was reformulated (corrected theory), and a numerical study of the pressure-drop characteristics of laminar flow of Newtonian fluids in sudden expansion geometries was undertaken.

The numerical predictions were carried out using a finite volume procedure based on second-order differencing schemes. The calculated values of the recirculating bubble length, the eddy strength and the location of the eddy centre matched available experimental and numerical data, when approximately fully developed conditions were imposed at inlet. The computed fully developed wall friction factors in the constant cross-section upstream and downstream pipes deviated less than 0.8% from the theoretical values.

The local loss coefficient in a 1:26 sudden expansion was predicted for inlet Reynolds numbers between 1 and 225 and compared with the theoretical values of the standard theory. The discrepancies between these two coefficients, which differed by more than 900% relative to the standard literature correlation at Reynolds numbers of the order of 1, were identified and quantified from the presented corrected-theory as:

(1) difference between the actual and the fully developed frictional loss of the walls;
(2) distortion of the velocity profile upstream of the expansion; and
(3) nonuniform pressure acting on the expansion plane.

At high-Reynolds number inertia-dominated flows, the frictional effect was the most important, of the order of 20% of the local loss coefficient, and the remaining effects were of opposite signs and of the order of 1.5%; whereas, at the low-Reynolds number viscous-dominated flows, the nonuniform pressure effect accounted for more than 80% of the coefficient.

After correcting the local loss coefficient based on the standard theory for the aforementioned effects, the differences between the corrected and predicted coefficients were less than 1% for Reynolds numbers above 17.5 and less than 4% for the Reynolds numbers between 1 and 17.5. In this range, the loss coefficient was found to be inversely proportional to the Reynolds number; whereas, it was approximately constant for Reynolds numbers above 17.5.

Finally, a correlation is proposed for the calculation of the local loss coefficient in the 1:2.6 sudden expansion as a function of the Reynolds number. Further work is currently under way to extend this equation to a wider range of Reynolds numbers and different expansion ratios.

Acknowledgments

The authors acknowledge the financial support of JNICT-Junta Nacional de Investigação Científica e Tecnológica, through contract number PBIC/P/QUI/1980/95.

References

Abbott, D. E. and Kline, S. J. 1962. Experimental investigation of subsonic turbulent flow over single and double backward-facing steps. *J. Basic Eng.*, **84**, 317–327

Back, L. and Roshke, E. 1972. Shear layer regimes and wave instabilities and reattachment lengths downstream of an abrupt circular channel expansion. *J. Appl. Mech.*, **94**, 677–681

Badekas, D. and Knight D. D. 1992. Eddy correlations for laminar axisymmetric sudden expansion flows. *J. Fluids Eng.*, **114**, 119–121

Batchelor, G. K. 1967. *An Introduction to Fluid Dynamics*. Cambridge University Press, Cambridge, UK, 1st edition, pp 373–376

Boger, D. V. 1981. Circular entry flows of inelastic and viscoelastic fluids. In *Advances in Transport Processes*, Wiley, New York, vol. 2, pp 43–98

Castro, I. P. 1979. Numerical difficulties in the calculations of complex turbulent flow. In *Turbulent Shear Flow I*, Durst et al. (eds.) Springer-Verlag, Berlin, Germany, 220

Drewry, J. E. 1978. Fluid dynamic characterization of sudden expansion ramjet combustor flow fields. *AIAA J.*, **16**, 313

Fletcher, D., Maskel, S. and Patrick, M. 1985. Heat and mass transfer computations for laminar flow in an axisymmetric sudden expansion. *Computers Fluids*, **13**, 207

Habib, M. A. and Whitelaw, J. H. 1982. The calculation of turbulent flow in wide-angle diffusers. *Numer. Heat Trans.* **5**, 145

Halmos, A. L. and Boger, D. V. 1975. The behavior of a power law fluid flowing through a sudden expansion. Part II. Experimental verification. *AIChEJ* **21**, 550–553

Halmos, A. L., Boger, D. V. and Cabelli, A. 1975. The behavior of a power law fluid flowing through a sudden expansion. Part I. Numerical solution. *AIChEJ*, **21**, 540–549

Idel'cik, I. E. 1971. *Memento des Pertes de Charge*. Editions Eyrolles, Paris, pp 109–126

Iribarne, A., Frantisak, F., Hummel, R. L. and Smith, J. W. 1972. An experimental study of instabilities and other flow properties of a laminar pipe jet. *AIChEJ*, **18**, 689–698

Khezzar, L., Whitelaw, J. H. and Yianneskis, M. 1985. An experimental study of round sudden expansion flows. *Proc. 5th Symposium on turbulent Shear Flows*, Cornell University, 5–25

Macagno, E. O. and Hung, T. K. 1967. Computation and experimental study of a captive annular eddy. *J. Fluid Mech.*, **28**, 43–64

McNaughton, K. J. and Sinclair, C. G. 1966. Submerged jets in short cylindrical flow vessels. *J. Fluid Mech.*, **25**, 367

Milos, F. and Acrivos, A. 1986. Steady flow past sudden expansion at large Reynolds number. Part I: Boundary-layer solutions. *Phys. Fluids*, **29**, 1353–1359

Monnet, P., Menard, C. and Sigli, D. 1982. Some new aspects to the slow flow of a viscous fluid through an axisymmetric duct expansion or contraction. II—Experimental part. *Appl. Sci. Res.*, **39**, 233–248

Oliveira, P. J. 1992. *Computer modelling of multidimensional multiphase flow and application to T-junctions*. Ph.D. thesis, Imperial College, University of London

Oliveira, P. J. and Pinho, F. T. 1995. Prediction of recirculating laminar flow in an axisymmetric sudden expansion. Internal rep. Dept. Electromecânica, Universidade da Beira Interior, Covilhã, Portugal and Dept. Eng. Mecânica e Gestão Industrial, Universidade do Porto, Portugal

Patankar, S. V. 1980. *Numerical Heat Transfer and Fluid Flow*. Hemisphere, Bristol, PA, pp 1–197

Perić, M. 1985. *A finite volume method for the prediction of three-dimensional fluid flow in complex duct*. Ph.D. thesis, Imperial College, University of London

Restivo, A. and Whitelaw, J. H. 1979. Instabilities in sudden expansion flows of relevance to room ventilation. *Proc. 2nd Symposium on Turbulent Shear Flow*, Imperial College, London, UK.

Scott, P., Mirza, F. and Vlachopoulos, J. 1986. A finite element analysis of laminar flows through planar and axisymmetric abrupt expansions. *Computers Fluids* **14**, 423–432

Stieglmeier, M., Tropea, C., Weiser, N. and Nitsche, W. 1989. Experimental investigation of the flow through axisymmetric expansions. *J. Fluids Eng.* **111**, 464–471.

Streeter, V. L. and Wylie, E. B. 1975. *Fluid Mechanics*, 6th ed., McGraw-Hill, New York, pp 1–585

Tadmor, Z. and Gogos, C. G. 1979. *Principles of Polymer Processing*, Wiley, New York, pp 1–692

White, F. M. 1979. *Fluid Mechanics*, McGraw-Hill, New York, 305–360